

We are IntechOpen, the world's leading publisher of Open Access books Built by scientists, for scientists

6,900

Open access books available

186,000

International authors and editors

200M

Downloads

Our authors are among the

154

Countries delivered to

TOP 1%

most cited scientists

12.2%

Contributors from top 500 universities



WEB OF SCIENCE™

Selection of our books indexed in the Book Citation Index
in Web of Science™ Core Collection (BKCI)

Interested in publishing with us?
Contact book.department@intechopen.com

Numbers displayed above are based on latest data collected.
For more information visit www.intechopen.com



Chapter

LDH Ternary Nanocomposites: g-C₃N₄ Intercalated ZnO\Mg-Al for Superior Photocatalytic Activity towards Dye Degradation

*Kandasamy Bhuvaneswari, Thangavelu Pazhanivel,
Govindasamy Palanisamy and Ganapathi Bharathi*

Abstract

Photocatalytic dye degradation has received more attention as an affordable and effective way to treat the dye polluted water. In the present chapter, we are going to discuss; (i) the preparation and photophysical characterization of g-C₃N₄ intercalated ZnO\Mg-Al LDH, a novel ternary nanocomposite, and (ii) its visible light photocatalytic degradation activity against the methylene blue dye. LDHs are 2D materials composed of “brucite-like” cationic layers where an inclusion of trivalent cations presents an overall positive charge to the nanosheets. g-C₃N₄ is one of the organic semiconductor photocatalyst which active for several types of reactions such as CO₂ reduction, water splitting, and degradation because of its stable, non-toxic, and earth-abundant nature. Mainly, the development of numerous 2D g-C₃N₄ nanosheets has been extensively used in the field of photocatalyst. By the combination heterojunction with 2D/2D interface can effectively improve the photocatalytic activity. The nitrogen-rich g-C₃N₄ intercalated ZnO\Mg-Al LDH ternary nanocomposite formation could follow the direct dye degradation process and results enhance the visible light absorption. The enhanced photocatalytic activity is mainly due to the improved charge separation rate and high number of photogenerated electrons. The large number of photogenerated electrons and high charge separation efficiency are effectively influence the dye degradation efficiency.

Keywords: layered double hydroxides, graphitic carbon nitride, photocatalytic activity, methylene-blue, ternary nanocomposites, visible light, dye degradation

1. Introduction

1.1 Water pollution

The industrial revolution could not avoid its effects on increasing environmental pollution, which pose a life threat to living beings. On the other hand, the increase of population rises the corresponding needs, which in turn result in the increased release of pollutants. The toxic substances from farmhouses, municipalities,

pesticides, and factories are the major sources of water pollution. Organic dyes are one of the major groups of pollutants which are released from textile industrial wastewater. The dye effluent contaminates the surface and groundwater, thereby, making it unfit for drinking and other daily usages. Polluted drinking water can cause serious cariogenic effects on human and other living beings.

The effective handling of increasing environmental pollution is a major challenge for the sustainable progress of modern civilization. With a lack of waste management measures, there is an urgent need in finding efficient ways to treat and decompose the pollutants. Water is a “universal solvent,” it can dissolve more substances than any other liquid on earth. It is because of this substantial property, water dissolves most of the pollutants and thus be polluted easily. Quality drinking water is a fundamental right to every human being and most of the countries do not provide drinking water in the WHO standards. Water pollution not only affects the human being, but also every living organism, as there is nothing without water.

Organic dyes used in many industries such as textiles, furniture, chemical, paint, food, and cosmetic industries are the major water pollutants. The organic dyes possess color owing to the following reasons; (i) the dye molecules absorb light in the visible region of the electromagnetic spectrum (400–700 nm), (ii) they have a conjugated structure, i.e. a structure with alternating single and double bonds, (iii) the molecule dye have at least one color bearing chromophore group, and (iv) exhibit resonance of electrons, which is a stabilizing force in organic compounds [1]. The removal of dye molecules is a challenging process because of the enormous variety of functional groups in dissimilar dyes and their different properties. Many techniques like electrochemical coagulation, reverse osmosis, nano-filtration, photocatalytic degradation, adsorption using activated materials etc., are used for the removal of dye from wastewater. Among the various types of approaches adsorption and photocatalytic degradation of chemically stable organic pollutants occupy a prominent place, due to some of the obvious advantages such as cost-effectiveness, simplicity of operation besides great efficiency.

1.2 Photocatalysis

Photocatalysis is a process, which accelerates a photoreaction in the presence of a photocatalyst. Photocatalysis, as a fresh, cheap, environmentally friendly “green” process, offers great potential for environmental protection and energy exchange. The organic pollutants can be effectively decomposed by the semiconductor-based photocatalysts under light irradiation with the photon energies equal or higher to the bandgaps of the photocatalysts. In recent years, the photocatalytic reaction has received increasing attention for environmental applications such as air purification, hazardous material remediation, water disinfection, and water purification. The versatility of the photocatalytic process, for example, photocatalytic degradation of dyes and photoelectrocatalytic reduction of CO₂ into hydrocarbon compounds in aqueous semiconductor suspensions, greatly attracted the scientists to work in the field of photocatalysis. The pioneering work of photo-electrochemical water splitting on TiO₂ electrode reported by Fujishima and Honda in 1972, has been the initiative in the field of photocatalysis. In this way, the semiconductor based photocatalysis has grown as an ideal green chemistry tool in dealing with the globally concerned energy shortage and environmental pollution issues. In general, a photocatalytic reaction consists of three simple steps; (i) The semiconductor photocatalysts absorb incident photons whose energy ($h\nu$) is equal to or more than its bandgap (E_g), resulting in the generation of electron-hole pairs, (ii) The photogenerated charge electrons and holes are separated and transferred to the surface of photocatalysts, and (iii) The photogenerated electrons and holes

contribute in catalytic reactions by forming superoxide and hydroxide radicals which react with dye molecules [2].

The detailed photocatalytic mechanism was shown in **Figure 1**. Several efforts have been conveyed through a variety of materials and methods and it is true, that each report put forward some scientific development to its ancestors. The photodegradation is one of the cost-effective and easy-to-implement methods, and the materials studied include TiO_2 , SnO_2 , ZnO , CuO , and WO_3 along with their heterostructures and organic/inorganic composites [3–7].

The photocatalytic decomposition of pollutants in the real-time application for water sanitation requires the use of non-toxic, cheap as well as reproducible resources. The conventionally used wide bandgap (SCs) with limited light responding range, which can only absorb UV light ($\lambda < 380$ nm), seriously confines the photocatalytic efficiencies. Therefore, it has become a significant problem to develop the photocatalytic SCs with a visible light response for practical applications. Besides, another major task in photocatalysis is the increase in the charge separation efficiency of the photocatalyst and the corresponding photocatalytic efficiency. The separation of the electron-hole pairs can increase the efficiency of photocatalysts. Transition metal oxides (TiO_2 , ZnO , SnO_2 , etc.) have lower photocatalytic efficiency since its wide bandgap and high recombination rate of photogenerated electron-hole pairs. To overcome this difficulty, the development of hetero-nanostructures could offer an enhancement in the photocatalytic efficiency and can act as a better photocatalyst which can degrade various kinds of persistent organic pollutants.

Among the numerous photocatalytic materials, ZnO occupied the reasonable research area owing to its whole beneficial characteristics over other materials [8, 9]. Even though, when it comes to commercial developments, the robustness of ZnO needs further developments [10]. Such as, the trapping state (including interstitial and missing atoms/vacancy defect) bolstered loss of excitons, which is basic in oxide-based semiconductors, should be tended to appropriately [11]. One plausibility of accomplishing this is, utilize a better surfactant/capping molecule to passivate the surface traps, which overwhelmingly trigger the charge carrier recombination. On the other hand, such passivation has the opportunity to acting as a barrier for hinders the association between the dye pollutant and active material, which will likewise bring low efficiencies. The development of a ZnO based hybrid photocatalyst comprising of a composite material with suitable band structure would be a better choice towards the concealment of charge carrier recombination and consequent improvement in the photocatalytic dye degradation process [12, 13].

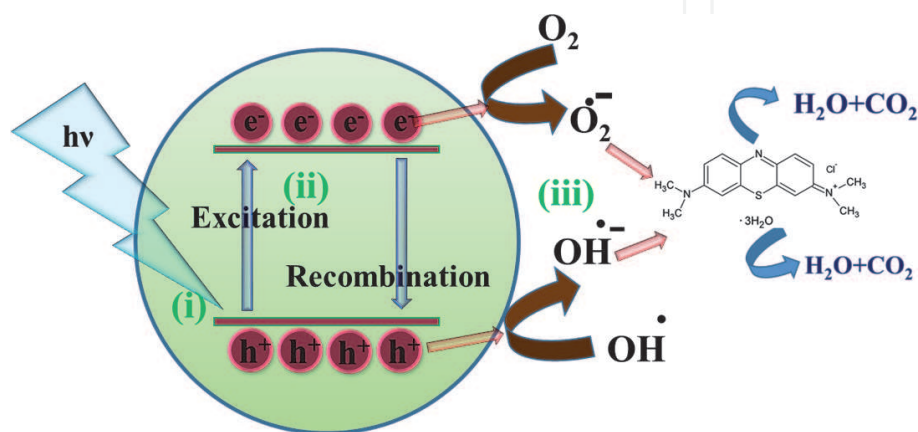


Figure 1.
Schematic illustration of photocatalytic dye degradation.

1.3 Graphitic carbon nitride (g-C₃N₄)

Graphitic carbon nitride (g-C₃N₄), is a two-dimensional metal-free conjugated crystalline sheet material with a bandgap energy of 2.7 eV, which has concerned exceptional research enthusiasm because of its environmental friendly nature, attractive electronic structure, low-cost excellent thermal and chemical stabilities [14–18]. The conduction and valence band boundaries of g-C₃N₄, exist at –1.12 and + 1.6 eV, making it active under visible light as an efficient photocatalyst [19–22]. Even though, its implication has drawbacks such as faster recombination of the electron-hole pairs, and agglomeration in most solvents caused by the strong van der Waals attractions between sp² carbon atoms [23]. 2D g-C₃N₄ nanosheets have much attention because of their enlarged specific surface area, improved electron–phonon interaction, and enhanced electron mobility along the in-plane direction [24]. Although some developments have been attained, the light-harvesting ability and quantum efficiency of these modified g-C₃N₄ systems are still poor.

For these reasons, various protocols such as surface modification, doping with metal or nonmetal elements and co-polymerization have been actively employed to enhance the photocatalytic performance of g-C₃N₄. It has high nitrogen content compared to other N-carbon materials, which is capable of creating more active reaction sites that would increase the electron donor/acceptor characteristics. Even after several decades and extensive investigations on several materials, a robust combination of materials and method is still required to vanish away the environment threatening organic pollutants.

1.4 Layered double hydroxides

Layered double hydroxides (LDH), a new class of lamellar metal hydroxide materials, consist of positively-charged hydrotalcite-like layers with carbonate ions and water molecules in the interlayer galleries [25–27]. Due to the two dimensional (2D) layered structure, LDH has a high explicit surface area, which can help quick ion transfer [26, 28–30]. Dvininov et al. prepared the SnO₂/Mg-Al LDH coupling through the thermal treatment, which demonstrated good photocatalytic activity for methylene blue degradation [31]. It was made conceivable by the oxygen reduction and progressive creation of hydroxyl radicals, which are accountable for the degradation. Seftel et al. synthesized Ti incorporated Mg-Al LDH solid which shows better photocatalytic activity due to the isolation of small TiO₂ nanoparticles on the LDH surface [32]. Kingshuk Dutta et al. prepared ZnO/Zn-Al LDH nanostructure by hydrothermal method using Al substrate as a template for developing different compositions and morphologies and the author demonstrated the degradation of Congo red dye [33]. Therefore, the LDH is a better candidate to be hybridized with ZnO which will enhance the catalytic activity of photocatalysts.

In any case, to build up a superior photocatalyst, hybridizing the LDH with a material having high conductivity and surface area is one of the hopeful approaches, which can further improve the charge transport proficiency of LDH-composite. Xiaoya Yuan et al. prepared the g-C₃N₄/Zn-Al LDH composites through a simple in situ crystallization technique and the as-prepared composite exhibited improved photodecolorization of MB.

In the present work, we have prepared a ternary nanocomposite of g-C₃N₄ intercalated ZnO/Mg-Al LDH through a hydrothermal technique and studied its photocatalytic activity against the MB dye degradation. The ZnO is attached on the surface also interlayers of the LDHs, and ZnO/Mg-Al LDH are distributed over the surface of g-C₃N₄ nanosheets. The nitrogen-rich ternary composite formation

resulted in the enhancement of visible light absorption and improved charge separation to result in the enhanced photocatalytic degradation activity towards the MB dye.

2. Experimental section

2.1 Preparation of $g\text{-C}_3\text{N}_4$ nanosheets

The $g\text{-C}_3\text{N}_4$ was prepared by a thermal condensation method using melamine as a precursor. 5 g of melamine was kept in an alumina crucible and thermally treated at 550°C for 3 h in a furnace. The obtained agglomerate residues are ground into fine powder and subjected to hydrochloric acid treatment for 12 h to obtain the $g\text{-C}_3\text{N}_4$ nanosheets. The suspension was centrifuged to separate the residual of $g\text{-C}_3\text{N}_4$ nanosheets. The obtained precipitate product was heated at 60°C for overnight to attain the light yellow colored powder of $g\text{-C}_3\text{N}_4$ nanosheets.

2.2 Preparation of Mg-Al LDH

In a typical synthesis procedure, Mg-Al LDH was prepared by a facile hydrothermal method. Firstly, 0.05 M of aluminum nitrate and 0.03 M of magnesium chloride were dissolved into 20 ml DDW separately under vigorous magnetic stirring for 10 min. Subsequently, 0.04 M of urea were dissolved into the 10 ml DDW and stirred for 30 min. After that, the precursor and urea solutions were mixed and 0.2 M of NaOH was added to the above solution mixture until the pH of the suspension was reached 12. The entire solution was transferred into a 100 ml Teflon lined stainless-steel autoclave, followed by heating in an oven under 180°C for 24 h. After the reaction was complete, the autoclave was cooled to room temperature. Finally, the sample was centrifuged and washed with DDW water and dried at 80°C for overnight to obtain the final product.

2.3 Preparation of ZnO nanoparticles

ZnO nanoparticles were prepared by the hydrothermal method. In this process, 0.2 M of ZnCl_2 were dissolved in 100 ml of DDW, and 0.2 M of NaOH were dissolved in 20 ml of DDW separately under constant stirring. After 10 min stirring the above-mentioned solutions were mixed together, and transferred into a 100 ml Teflon liner stainless-steel autoclave, followed by heating in an oven under 180°C

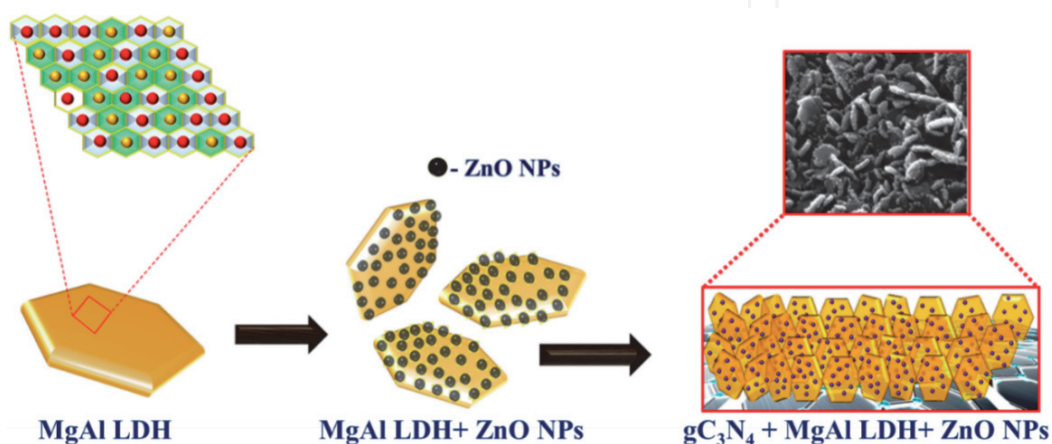


Figure 2.
Pictorial representation for the formation of $g\text{-C}_3\text{N}_4/\text{ZnO}/\text{Mg-Al LDH}$ 2D/2D LDH tertiary nano-composite [34].

for 24 h. Later, the autoclave was cooled down naturally. Finally, the obtained solution was centrifuged and washed with DDW water and dried at 80°C for overnight to obtain the final product.

2.4 Preparation of 2D\2D hybrid

A certain amount of g-C₃N₄ was dispersed into 20 ml of DDW and ultrasonicated for 30 min. Subsequently, the ZnO\Mg-Al precursor solution was prepared and mixed with ultrasonicated g-C₃N₄ nanosheets. Again, the mixture was ultrasonicated for 30 min in a beaker to form a homogeneous suspension. After that, the reaction mixture was transferred into a 100 ml Teflon liner stainless-steel autoclave, followed by heating in an oven under 180°C for 24 h. After that, the autoclave was cooled down naturally to ambient temperature. Finally, the sample was centrifuged and washed with DDW water and dried at 80°C for overnight to obtain the final product. **Figure 2** shows the formation of g-C₃N₄\ZnO\Mg-Al LDH 2D\2D hybrid.

3. Characterization details

The photocatalytic activities mostly depend on the material nature, specific surface area, and light energy utilization ratio [35] etc., and for these reasons the crystallinity, functional group, surface area morphology and photophysical properties of the as-prepared samples were systematically investigated by various analytical techniques.

- i. Structural investigation
- ii. Morphology analysis
- iii. Elemental analysis
- iv. Photophysical investigation
- v. Surface area investigation

3.1 Structural investigation

The crystalline phases have a significant influence on the photocatalytic activities [36]. So the phase purity and crystallite size of the synthesized samples were evaluated by X-ray diffractometer using Rigaku MiniFlux-II diffractometer using Cu K α radiation ($\lambda = 1.54046 \text{ \AA}$). The crystalline nature of the prepared samples were investigated through XRD analysis and **Figure 3** displays the XRD pattern of Mg-Al LDH, gC₃N₄, ZnO and g-C₃N₄\ZnO\Mg-Al LDH ternary nanocomposite.

The XRD pattern of the Mg-Al LDH and g-C₃N₄, sample is in good agreement with the JCPDS card no: 35-0965 [37] and 87-1526 [38], respectively. The diffraction peaks indexed to (003), (006), (012), (015), (018), and (110) are the plane reflections of a typical hydrotalcite-like phase screening, sharp and symmetric basal (00 l) reflection of LDH. The XRD pattern of ternary nanocomposite consists of g-C₃N₄, ZnO and Mg-Al LDH diffraction peaks indicate the formation of the composite.

3.2 Morphological analysis

3.2.1 FE-SEM analysis

The surface morphology of the prepared samples was investigated by using FESEM and HRTEM analyses, respectively. The FE-SEM images were obtained by using Zeiss SUPRA-25 and the particle size and morphology of the prepared samples were analyzed by using HR-TEM – Jeol/JEM 2100, with LaB6 source.

Figure 4 shows the FESEM images of (a) Mg-Al LDH, (b) $g\text{-C}_3\text{N}_4$, (c) ZnO and (d) $g\text{-C}_3\text{N}_4$ \ZnO\Mg-Al LDH ternary nanocomposite samples. The Mg-Al LDH consists of plenty of two-dimensionally structured hexagonal LDHs matrix with a layer by layer assembly. The size of the hexagonal nanoflakes is approximately 200 nm, which indicate the successful exfoliation of a 2D layer.

3.2.2 HRTEM analysis

Furthermore, the hexagonal formed hydroxide-like particles were seen from the HRTEM analysis (**Figure 4d** and **e**) and it concurs well with the morphology

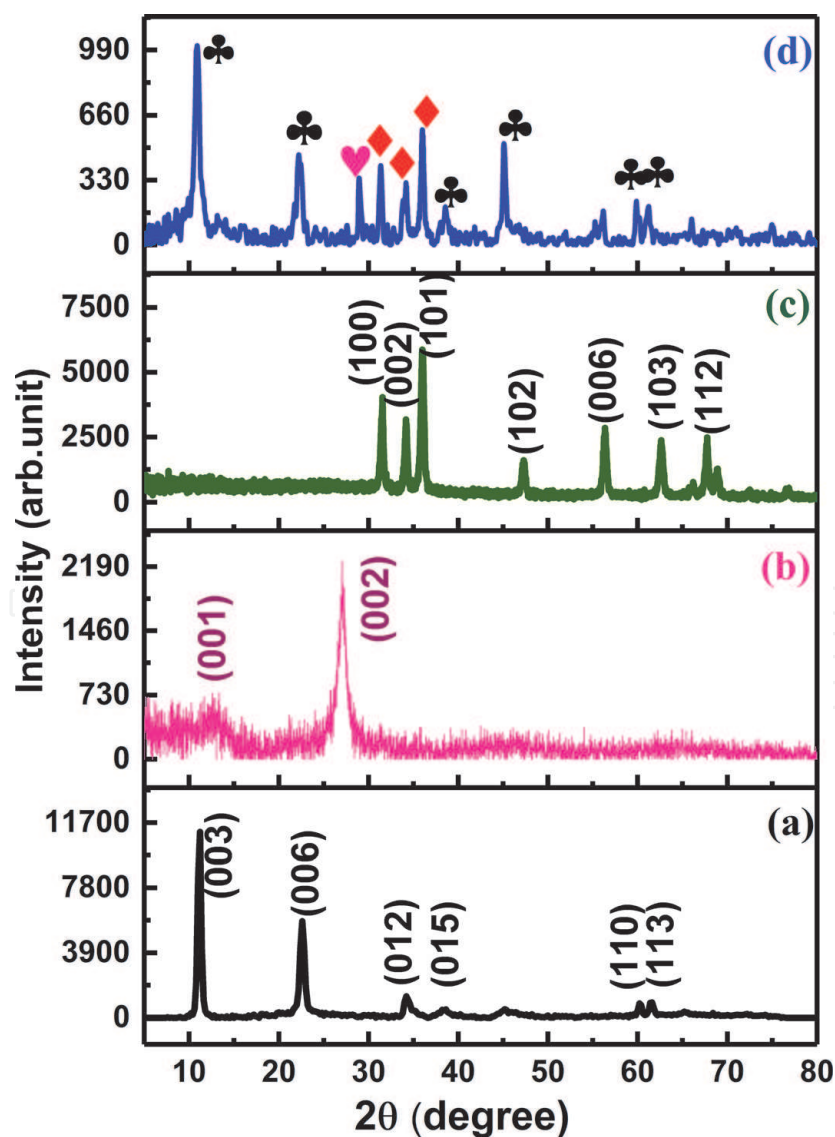


Figure 3. XRD pattern of (a) Mg-Al LDH, (b) $g\text{-C}_3\text{N}_4$, (c) ZnO and (d) $g\text{-C}_3\text{N}_4$ \ZnO\Mg-Al LDH ternary nanocomposite [34].

acquired from FE-SEM investigation. Some dull spots showed up on the outside of the LDH, demonstrating that the ZnO nanoparticles are well attached on the LDH surfaces. Some dark spots appeared on the surface of the LDH, indicating that the ZnO nanoparticles are well attached to the surface of the as-prepared LDH. The 2D\2D ternary nanocomposites assembly was successfully obtained, and by arresting the ZnO\Mg-Al LDH sheets with g-C₃N₄ sheets, the formation of the 2D\2D ternary nanocomposite was possible. Surprisingly, after the formation of the ternary nanocomposite, the LDH loose its horizontal stacking arrangements and started aligning vertically on the surface of the g-C₃N₄ nanosheets. These types of arrangements provide a more active surface for the prepared photocatalysts.

3.3 Chemical analysis

The surface chemical composition of the prepared samples was confirmed by the FTIR, EDAX, Elemental mapping, and XPS analyses.

3.3.1 FTIR analysis

The vibrational bands of the prepared samples were analyzed by FTIR analysis (using a Bruker model Tensor 27 instrument) and the results are shown in **Figure 5a**. All the spectra, exhibit a strong band at 3700 to 3000 cm⁻¹ which could be ascribed to the vibration of surface adsorbed water molecules and in the case of LDH plates, it is due to the formation of interlayer water molecules. Furthermore, several bands were observed in the 1200–1650 cm⁻¹ region, which is assigned to the characteristic stretching modes of C—N heterocycles [39]. The absorption bands at 1620 cm⁻¹ are associated with the C=O of the carboxylate groups. The occurrence of the feeble band at 1631 and 1643 cm⁻¹ can be ascribed to the bending frequency and O—H asymmetric stretching vibration of the water molecules, respectively [40, 41]. The characteristic absorption band of ZnO samples was observed at 595 cm⁻¹, which is related to the metal-oxygen stretching vibration. The absorption

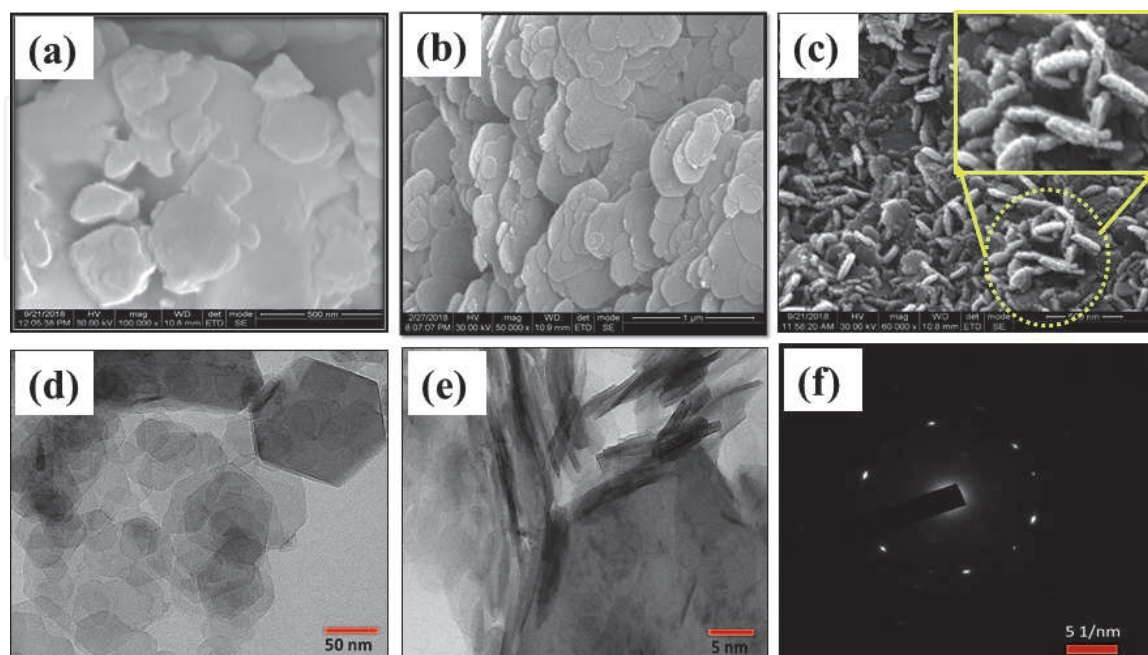


Figure 4. Morphology analysis: FE-SEM images of (a) Mg-Al LDH, (b) g-C₃N₄, (c) g-C₃N₄/ZnO/Mg-Al LDH ternary nanocomposite and HRTEM images of (d) Mg-Al LDH, (e) g-C₃N₄/ZnO/Mg-Al LDH ternary nanocomposite, (f) SAED pattern of ternary nanocomposite [34].

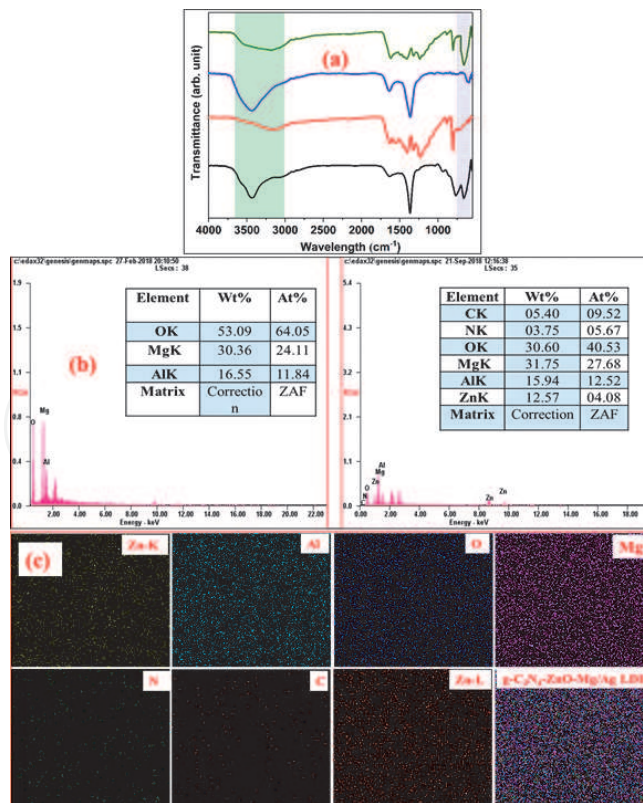


Figure 5. (a) FTIR spectra for as prepared samples (b) EDX spectra of MgAl LDH and $g\text{-C}_3\text{N}_4/\text{ZnO}/\text{Mg-Al}$ LDH ternary nanocomposite and (c) mapping analysis of $g\text{-C}_3\text{N}_4/\text{ZnO}/\text{Mg-Al}$ LDH ternary nanocomposite [34].

bands at 653 cm^{-1} could be owed to the M—O—M lattice vibrations of the hexagonal sheets [42]. The successful intercalation of $g\text{-C}_3\text{N}_4$ and ZnO with Mg-Al LDH were observed from the presence of their corresponding bonds, in the FTIR results.

3.3.2 EDX analysis

Figure 5b shows the observed elemental composition of the ternary nanocomposite by EDX analysis (carried out using a JEOL Model JED 2300). From the EDX results, it could be able to observe the high percentages of O, Mg and Al elements, present in the as-prepared samples and no other impurities were observed. The elemental mapping of Mg-Al LDH and $g\text{-C}_3\text{N}_4/\text{ZnO}/\text{Mg-Al}$ LDH ternary nanocomposite were presented in **Figure 5c**, which indicates the even distribution of the observed elements across the sample.

3.3.3 XPS analysis

XPS analysis was used to investigate the surface chemical composition of the prepared ternary nanocomposite and the obtained results were shown in **Figure 6**. The survey spectra show that the prepared sample is contain Mg, Al, Zn, O, C and N elements which creating peaks corresponding to Mg 1s, Al 2p, Zn 2p, O 1s, C 1s, and N 1s positions, respectively (**Figure 6A**). The high-resolution spectra of individual elements are presented in **Figure 6B**. The Mg^{2+} species are observed by the presence of Mg 2p, Mg 2s, Mg KLL, and Mg 1s state corresponding to the binding energies of 52.8, 90.8, 306.8, 351.8 and 1302.8 eV, respectively [43]. The high-resolution spectra of Mg 1s are fitted with three segments associating to the binding energies of 1307, 1308 and 1308.8 eV, which are ascribed to Mg, Mg-CO_3 and MgO [44, 45]. The Al attributed to the two states such as Al 2p and Al 1s and the characteristic

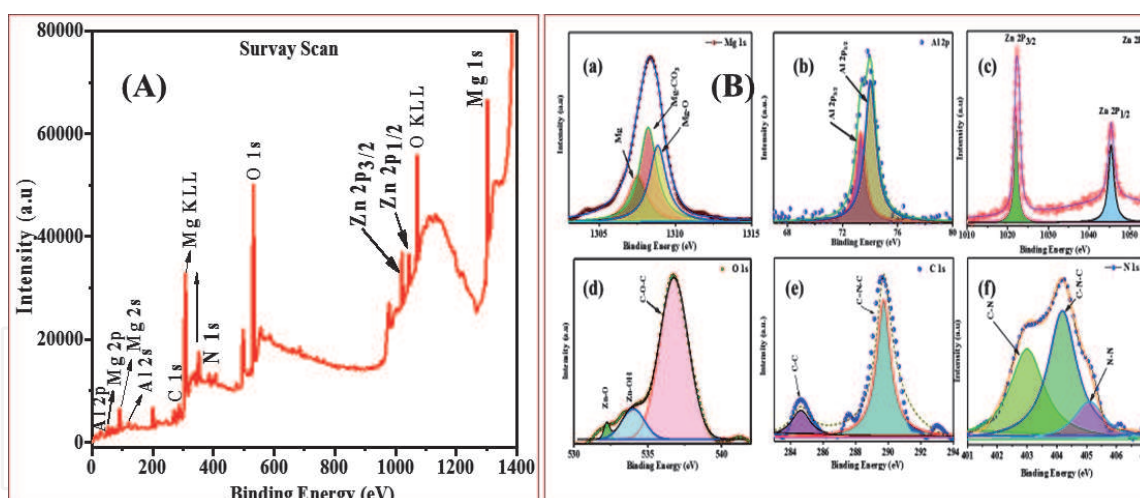


Figure 6.

XPS spectra of $C_3N_4/ZnO/Mg-Al$ LDH ternary nanocomposite: (A) survey spectra and (B) high resolution XPS spectra of (a) Mg 1s (b) Al 2p (c) Zn 2p (d) O 1s (e) C 1s (f) N 1s [34].

peak were observed at 76.8 and 120.8 eV. The occurrence of Zn is seen from the two Zn 2p states as Zn 2P_{3/2} and Zn 2P_{1/2} corresponding to 1020.8 and 1043.8 eV respectively. It additionally uncovers that the Zn is available just in 2⁺ oxidation state which affirms the conceivable bonding between Zn and O [10]. The oxygen O 1s is deconvoluted into three peaks corresponding to the O²⁻ at 532.2 eV, OH⁻ species at 533 eV and C—O—O at 536 eV, respectively [46]. In over-all, the inferior binding vitality of O 1s peaks emerges from the bond between O²⁻ and Zn²⁺ metal ions. The C 1s spectra can be deconvoluted into dual contributions such as 284.4 and 289 eV, assigned to the occurrence of sp² hybridized carbon atoms and C=N—C bonding [47], respectively. The N 1s spectra can be tailored into three basic peaks with the binding energies of 402, 404.1 and 405 eV, which are attributable to the binding of C—N, C—N—C, and N—N respectively [20]. Henceforth, the above observations affirm the formation of g-C₃N₄/ZnO/Mg-Al LDH ternary nanocomposite and the XPS results are in good agreement with FTIR, EDX and mapping analyses.

3.4 Photophysical investigation

3.4.1 UV-Vis absorption spectra

Optical properties possess a prominent role in the photocatalytic materials and therefore the photophysical properties of the prepared materials were investigated by UV-Vis and PL analyses. The optical absorption analysis was done using a SHIMADZU 3600 UV-Vis-NIR spectrophotometer and Emission spectrum of the as-prepared samples was recorded by using Horiba Jobin Yvon Spectro Fluomax 4. **Figure 7A** shows the UV-Vis. absorption spectra of the prepared samples. The absorption maxima were observed in the range between 320 and 450 nm. And the absorption of ternary nanocomposite was extended to the visible region and show an obvious red shift compared with the other samples, which may because of the interaction between the ZnO, LDH, and g-C₃N₄. The 2D\2D formation demonstrates a reality that the as-prepared ternary nanocomposite noticeable light vitality which can thusly create more charge transporters offered to contribution in the photocatalytic efficiency. Tauc's plot was used to determine the energy bandgap of the samples and the obtained values are 2.6, 3.5, 2.57 and 2.81 eV for LDH, ZnO,

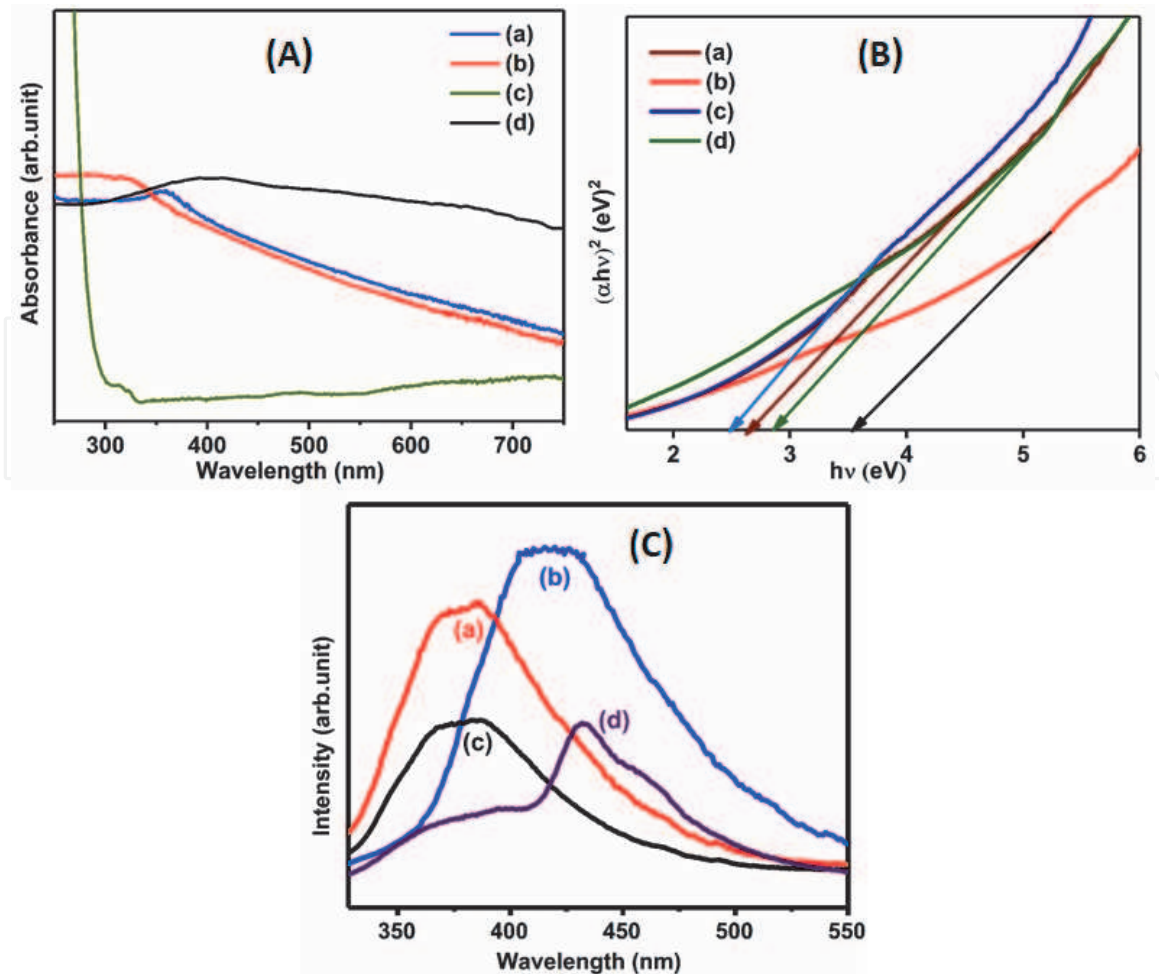


Figure 7. (A) UV-Vis absorption spectra (B) Tauc's plots and (C) PL spectra of the prepared samples ((a) Mg-Al LDH and (b) ZnO (c) $g\text{-C}_3\text{N}_4$ (d) $g\text{-C}_3\text{N}_4/\text{ZnO}/\text{Mg-Al}$ LDH ternary nanocomposite) [34].

$g\text{-C}_3\text{N}_4$, $g\text{-C}_3\text{N}_4/\text{ZnO}/\text{Mg-Al}$ LDH ternary nanocomposite, respectively. The UV-Vis absorption results show the considerable enhancement in the visible light absorption and it is because of this reason, an enhancement in the photocatalytic performance of the as-prepared photocatalyst is observed (discussed in the latter part).

3.4.2 PL spectra

The emission spectrum is produced because of recombination of the charge carriers and it provides hints about the proficiency of charge carrier transformation, trapping, and separation of the photo generated electrons-holes pairs. The strong PL emission profile usually indicates the quick recombination of electron-hole pairs which provides low photocatalytic activity.

Figure 7C shows the PL emission spectra of (a) MgAl LDH, (b) $g\text{-C}_3\text{N}_4$, (c) ZnO and (d) $g\text{-C}_3\text{N}_4/\text{ZnO}/\text{Mg-Al}$ LDH ternary nanocomposite, which were recorded using 320 nm as excitation wavelength. The LDH and ZnO nanoparticles exhibit a strong PL emission in the range from 350 to 450 nm. The pure $g\text{-C}_3\text{N}_4$ shows a strong emission about ~ 420 nm, which can be attributed to the fast electron-hole recombination process. It can be seen that, after the formation of ternary nanocomposite the emission intensity was decreased which may be due to the delocalization of electrons. In general, a decrease in the recombination rate gives rise to a low PL intensity, which results in the maximum photocatalytic activity.

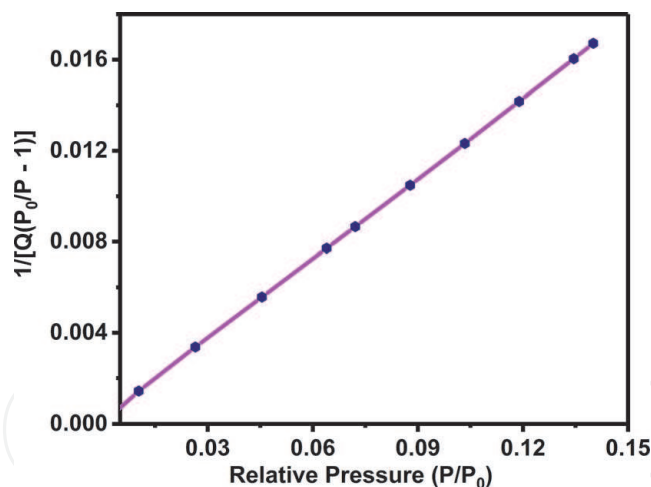


Figure 8. BET surface area analysis of $g\text{-C}_3\text{N}_4/\text{ZnO}/\text{Mg-Al}$ LDH ternary nanocomposite [34].

3.5 Surface area investigation

The specific surface area of the photocatalyst was determined by Brunauer-Emmett-Teller (BET) analysis through N_2 adsorption/desorption measurements at 25°C (Figure 8). The measured surface area of the ternary nanocomposite was $\sim 37 \text{ m}^2 \text{ g}^{-1}$. The high surface area support more active species and reactants to be absorbed on its surface, which might proficiently help the kinetics of photo catalytic reaction.

4. Photocatalytic activity

4.1 Dye removal procedure

The photocatalytic activity of the as-prepared samples was investigated under UV-Vis light irradiation. The aqueous MB solution (20 mg L^{-1}) was prepared and kept in dark for 60 min to attain equilibrium. Later, 10 mg of the as-prepared photocatalyst was added to 10 ml MB solution and it was placed in a water jacketed photocatalytic reactor for the photocatalytic degradation process. A 250 W Hg lamp was used as the illumination source to excite the photocatalysts. In the whole reaction, the photocatalytic container was maintained at room temperature by circulating water. At 15 min time interval, 3 ml of solution was taken and centrifuged to remove the photocatalyst particles. The supernatant was examined by a Shimadzu UV3000 UV-Vis spectrophotometer and the dye absorption band maximum was observed at $\sim 664 \text{ nm}$. The percentage of degradation was calculated using the Beer-Lambert relation [48]:

$$A(\lambda) = \log(I(\lambda)/I_0(\lambda)) = -\epsilon l[\text{BM}] \quad (1)$$

where

A – absorbance at a given wavelength λ ,

$I_0(\lambda)$ – incident light intensity,

$I(\lambda)$ – light intensity transmitted through the MB solution,

ϵ – Molar attenuation coefficient of MB.

l – Path length of the beam of light.

The degradation efficiency was calculated by

$$\text{Degradation (\%)} = (C_0 - C) \backslash C_0 * 100 \quad (2)$$

where,

C_0 is the initial dye concentration and

C is the dye concentration at time t from the start of the photocatalytic reaction.

For the reusability purpose, the as-prepared photocatalyst collected after the photocatalytic reaction by centrifuging, washed with DDW and then dried at 60°C .

4.2 Radical trapping experiment

To elucidate the reaction mechanism of the photocatalytic MB dye degradation, the radical trapping investigation was performed. In the scavenging activity, h^+ , OH and O_2^- radicals are trapped by EDTA, 2-propanol and benzoquinone, respectively. The trapping experiments were carried out with the accumulation of different scavengers into the catalytic reaction. The reaction samples were taken from the photocatalytic reactor to record their UV-Vis absorption spectra.

4.3 Reaction mechanism of dye degradation

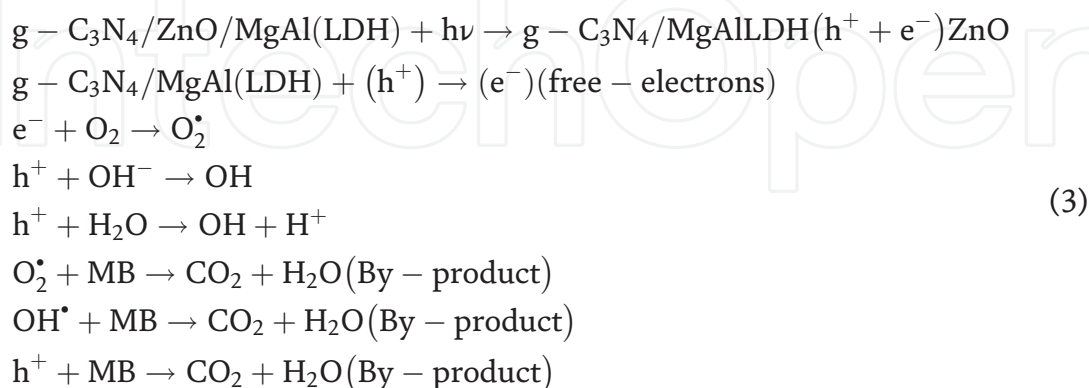
The photocatalytic activities of the Mg-Al LDH, $g\text{-C}_3\text{N}_4$, and $g\text{-C}_3\text{N}_4\backslash\text{ZnO}\backslash\text{Mg-Al}$ LDH ternary nanocomposite were assessed under UV-Vis light illumination. In this work, MB dye was utilized as an objective contamination so as to decide the photocatalytic action of the impetuses under obvious light illumination. The MB dye solutions were prepared and the photocatalytic reactions were performed by adding the as-prepared samples to the MB dye solutions. The pure MB dye fragment shows a strong visible light absorption around 664 nm. The MB dye with prepared photocatalyst is subjected under the visible light irradiation, corresponding absorption peak intensity was decreased, and the decreasing MB dye intensity is attributed to the degradation of MB dye through the photocatalytic activity. When increases the irradiation time, absorption intensity of MB dye molecules was decreased (i.e.) once increase the irradiation/reaction time, the large number of dye molecules can be degraded. In this process, a photocatalyst is irradiated by light with energy equal to or higher than the bandgap energy of the photocatalyst. This results in the excitation of an electron (e^-) from the valence band to the conduction band, leaving a hole (h^+) in the valence band. Before the recombination takes place, the photogenerated electrons (e^-) and holes (h^+) should be transferred to the surface of the photocatalyst in order to take part in the redox reactions with the adsorbed species. The redox reactions of electrons (e^-) and holes (h^+) with adsorbed oxygen and water molecules lead to the formation of superoxide radical anion ($^{\bullet}\text{O}_2^-$) and hydroxyl radical ($^{\bullet}\text{OH}$), respectively.

Among all the as-prepared photocatalyst samples, $g\text{-C}_3\text{N}_4\backslash\text{ZnO}\backslash\text{Mg-Al}$ LDH ternary nanocomposite sample exhibit better photocatalytic activity. This could be attributed to a large number of electrons and holes generated by the as-prepared photocatalyst system, caused by the favorable visible light absorption. On the other hand, ZnO, a wide bandgap material, provides intermediate states to delay the electron-hole recombination, which could also contribute to the high photocatalytic activity. The morphological arrangements of the nanocomposite and its resultant electronic structure, (i.e.) the even distribution of ZnO intercalated LDH over the surface of $g\text{-C}_3\text{N}_4$ [49], collectively contribute to the effective separation of the photogenerated charge carriers. The observed photocatalytic degradation efficiencies of the as-prepared photocatalysts are 32%, 30%, 49% and 96.5% for ZnO, LDH, $g\text{-C}_3\text{N}_4$, and $g\text{-C}_3\text{N}_4\backslash\text{ZnO}\backslash\text{Mg-Al}$ LDH ternary nanocomposite, respectively.

It has to be noted that the photocatalytic efficiency reported in the present study, better our previous research work, in which ZnS QDs-LDH [49] exhibited a photocatalytic degradation efficiency of 95%. The enhanced photocatalytic efficiency is originated from the photocatalytic activity of N-rich g-C₃N₄, (i.e.,) the improved photocatalytic mechanism could be ascribed to the synergetic effect of graphitic N rich surface which offers more reactive sites for photocatalytic reaction. This in turn increases the utilization of the photo-separated charges towards the radical formation and corresponding degradation. Parallely, the N-carbon acted as a co-catalyst to improve surface reaction kinetics and the nitrogen species directly contributed to the outstanding photocatalytic activity under visible light irradiation. Especially the nitrogen rich surface can achieve essential optical absorbance under visible light due to the mixing of O 2p states with p states. And also the nitrogen rich surface 2D/2D offers more active surface for the e⁻ transfer. The reaction kinetics of the MB dye degradation of the prepared photocatalysts is investigated by fitting the pseudo-first-order kinetic curve [50].

The plots of ln (C₀\C) against illumination time are appeared in **Figure 9**. From the kinetic graph, the ternary nanocomposite fits well and the outcome is in concurrence with the pseudo-first-order model. The impact of different scavengers on the photodegradation of MB dye solution was studied in order to recognize the role of receptive oxidative species in the photodegradation process. The role of H⁺, OH and O₂ radicals were done individually, utilizing EDTA, 2-propanol, and BQ respectively. During the addition of EDTA and BQ, there were conspicuous variations in the photocatalytic process, which shows that H⁺ and O₂ radicals are influences in MB dye degradation. But after the addition of 2-Propanol (scavenger for the OH radical), the degradation of MB is highly suppressed than other reactions, indicating the major of *OH in MB dye degradation. From this result, it is clear that the photocatalytic degradation process is led by the contribution of hydroxyl radical (*OH). After the addition of the as-prepared photocatalyst into the reaction and irradiating with visible light, the electrons were photoexcited from the valence band (VB) to the conduction band (CB). Once electrons are excited, the hole act as an oxidizing agent and oxidize the aquatic or the dye directly to form *OH radicals.

These OH reactive species are responsible for the efficient degradation of organic pollutants in water. The following equation represent the possible photocatalytic reaction mechanism of MB dye degradation under visible light irradiation.



The **Figure 10** shows the schematic illustration of possible photocatalytic degradation of MB dye under visible light irradiation. The reusability of the prepared photocatalyst was studied by performing continual tests under same reaction conditions (shown in **Figure 11b**). The fresh MB solution was utilized for resulting cycles. Subsequently in each cycle, the prepared catalyst was isolated from the photocatalytic reactor through centrifugation. After 4 cycles, the degradation ability of the prepared catalyst was slightly reduced and it might be because of the loss

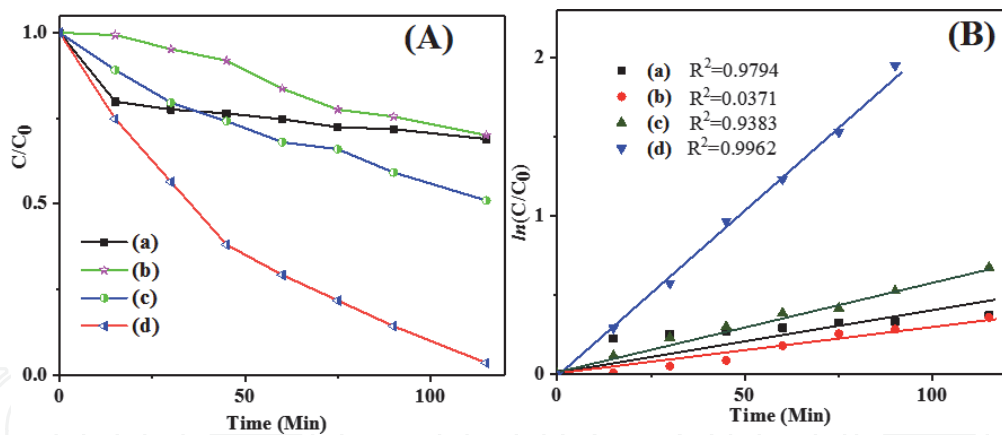


Figure 9. (A) Photocatalytic degradation and (B) pseudo-first-order kinetics for the degradation of MB over (a) ZnO (b) LDH (c) $g\text{-C}_3\text{N}_4$ (d) $g\text{-C}_3\text{N}_4\backslash\text{ZnO}\backslash\text{Mg-Al}$ LDH ternary nanocomposite [34].

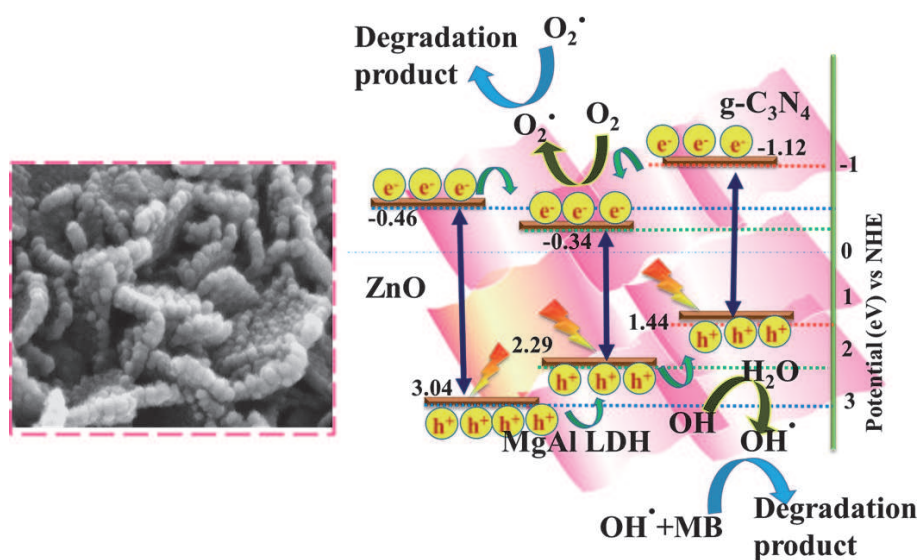


Figure 10. Schematic illustration of proposed photocatalytic reaction mechanism.

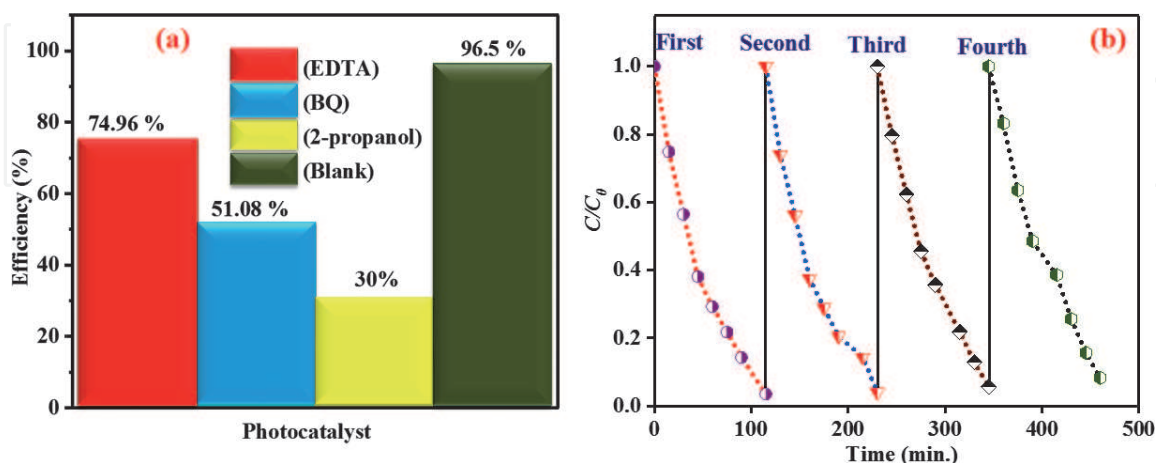


Figure 11. (a) Radical trapping experiments of active species over $g\text{-C}_3\text{N}_4\backslash\text{ZnO}\backslash\text{Mg-Al}$ LDH ternary nanocomposite and (b) reusability of $g\text{-C}_3\text{N}_4\backslash\text{ZnO}\backslash\text{Mg-Al}$ LDH ternary nanocomposite in the photodegradation of MB [34].

of catalyst during the recycling process. The photocatalytic dye degradation activity of the prepared sample was compared to the previously reported nanomaterials, which is given in **Table 1**.

S. No	Catalyst	Dosage of dye (mg)	Dye	Light source	Catalyst efficiency (%)	Reaction time (min)	References
1.	PANI-ZnO	100	MB	250 W	98.3	180	[51]
2.	Nitrogen doped dual phase titanate	10	MB	450 W	~97	310	[52]
3.	Zirconia	50	MB	500 W	~78	300	[53]
4.	CA-CNT/TiO ₂ -NH ₂	2 cm × 13 cm (CNT)	MB	40 W	80	300	[54]
5.	TiO ₂	100	MB	6 W	97	180	[55]
6.	g-C ₃ N ₄ /ZnO/Mg-Al LDH	10	MB	250 W	96.5	120	Present work

Table 1.

Comparison table of MB dye degradation using different photocatalyst with degradation (%) of previously reported nanomaterials.

Form the experimental results, it was confirmed that the as-prepared ternary nanocomposite exhibits remarkable photocatalytic activity and reusability under visible light to photo-degrade MB dye.

5. Conclusion

In summary, the hydrothermally prepared 2D\2D ternary nanocomposite was used as an efficient photocatalyst for the photodegradation of MB dye. The nitrogen-rich 2D\2D (g-C₃N₄ and Mg-Al LDH) surface significantly enhanced the photocatalytic efficiency under the visible light irradiation due to the improved photo active surfaces. Especially, in ternary nanocomposite Mg-Al LDH 2D nanoplates are vertically well aligned on the surface of the g-C₃N₄ 2D nanosheets. This 2D/2D arrangement results effectively enhances the photocatalytic activity due to the efficient separation of photo-induced charge carriers and transfer by the incorporation of ZnO into LDH brucite layers. In addition, the g-C₃N₄ surface contributed to the efficient charge injection in the photocatalytic reaction. The novel g-C₃N₄/ZnO/Mg-Al LDH ternary nanocomposite can be used as a proficient material for the photocatalytic degradation of MB dyes under visible light irradiation.

6. Future aspects/prospective

1. The as prepared ternary nanocomposite show large specific surface area and efficiently active in the visible light region so this material can used as a good photocatalytic for other organic dye degradation
2. The LDH have large number of interlayer galleries which can capable to adsorb the pollutants such as heavy metals synthetic or organic dyes.

IntechOpen

Author details

Kandasamy Bhuvaneshwari¹, Thangavelu Pazhanivel^{1*}, Govindasamy Palanisamy¹
and Ganapathi Bharathi²

¹ Smart Materials Interface Laboratory, Department of Physics, Periyar University,
Salem, Tamilnadu, India

² Key Laboratory of Optoelectronic Devices and Systems of Guangdong Province,
College of Optoelectronic Engineering, Shenzhen University, Shenzhen,
Guangdong Province, P.R. China

*Address all correspondence to: pazhanit@gmail.com

IntechOpen

© 2020 The Author(s). Licensee IntechOpen. This chapter is distributed under the terms of the Creative Commons Attribution License (<http://creativecommons.org/licenses/by/3.0>), which permits unrestricted use, distribution, and reproduction in any medium, provided the original work is properly cited. 

References

- [1] Axelson SO. IARC monographs on the evaluation of carcinogenic risks to humans. IARC Monographs on the Evaluation of Carcinogenic Risks to Humans. 2010;**94**:9-38
- [2] Sun W, Meng S, Zhang S, Zheng X, Ye X, Fu X, et al. Insight into the transfer mechanisms of Photogenerated carriers for heterojunction photocatalysts with the analogous positions of valence band and conduction band: A case study of ZnO/TiO₂. *Journal of Physical Chemistry C*. 2018;**122**:15409-15420. DOI: 10.1021/acs.jpcc.8b03753
- [3] Prabhu S, Pudukudy M, Sohila S, Harish S, Navaneethan M, Navaneethan D. Synthesis, structural and optical properties of ZnO spindle/reduced graphene oxide composites with enhanced photocatalytic activity under visible light irradiation. *Optical Materials*. 2018;**79**:186-195. DOI: 10.1016/j.optmat.2018.02.061
- [4] Nakata K, Fujishima A. TiO₂ photocatalysis: Design and applications. *Journal of Photochemistry and Photobiology C Photochemistry Reviews*. 2012;**13**:169-189. DOI: 10.1016/j.jphotochemrev.2012.06.001
- [5] Prakash K, Senthil Kumar P, Pandiaraj S, Saravanakumar K, Karuthapandian S. Controllable synthesis of SnO₂ photocatalyst with superior photocatalytic activity for the degradation of methylene blue dye solution. *Journal of Experimental Nanoscience*. 2016;**11**:1138-1155. DOI: 10.1080/17458080.2016.1188222
- [6] Kim SP, Choi MY, Choi HC. Photocatalytic activity of SnO₂ nanoparticles in methylene blue degradation. *Materials Research Bulletin*. 2016;**74**:85-89. DOI: 10.1016/j.materresbull.2015.10.024
- [7] Lee KM, Lai CW, Ngai KS, Juan JC. Recent developments of zinc oxide based photocatalyst in water treatment technology: A review. *Water Research*. 2016;**88**:428-448. DOI: 10.1016/j.watres.2015.09.045
- [8] Guo M, Diao P, Cai S. Hydrothermal growth of perpendicularly oriented ZnO nanorod array film and its photoelectrochemical properties. *Applied Surface Science*. 2005;**249**:71-75. DOI: 10.1016/j.apsusc.2004.11.053
- [9] Jalal R, Goharshadi EK, Abareshi M, Moosavi M, Yousefi A, Nancarrow P. ZnO nanofluids: Green synthesis, characterization, and antibacterial activity. *Materials Chemistry and Physics*. 2010;**121**:198-201. DOI: 10.1016/j.matchemphys.2010.01.020
- [10] Thirumalai K, Shanthi M, Swaminathan M. Hydrothermal fabrication of natural sun light active Dy₂WO₆ doped ZnO and its enhanced photo-electrocatalytic activity and self-cleaning properties. *RSC Advances*. 2017;**7**:7509-7518. DOI: 10.1039/c6ra24843h
- [11] Raza W, Faisal SM, Owais M, Bahnemann D, Muneer M. Facile fabrication of highly efficient modified ZnO photocatalyst with enhanced photocatalytic, antibacterial and anticancer activity. *RSC Advances*. 2016;**6**:78335-78350. DOI: 10.1039/c6ra06774c
- [12] Yuan G, Xiang J, Jin H, Wu L, Jin Y, Zhao Y. Anchoring ZnO nanoparticles in nitrogen-doped graphene sheets as a high-performance anode material for lithium-ion batteries. *Materials*. 2018;**11**:15-17. DOI: 10.3390/ma11010096
- [13] Zhang L, Li L, Sun X, Liu P, Yang D, Zhao X. ZnO-layered double hydroxide@graphitic carbon nitride composite for consecutive adsorption

and photodegradation of dyes under UV and visible lights. *Materials*. 2016;**9**:11. DOI: 10.3390/ma9110927

[14] Zhao Y, Zhao F, Wang X, Xu C, Zhang Z, Shi G, et al. Graphitic carbon nitride nanoribbons: Graphene-assisted formation and synergic function for highly efficient hydrogen evolution. *Angewandte Chemie, International Edition*. 2014;**53**:13934-13939. DOI: 10.1002/anie.201409080

[15] Xu C, Han Q, Zhao Y, Wang L, Li Y, Qu L. Sulfur-doped graphitic carbon nitride decorated with graphene quantum dots for an efficient metal-free electrocatalyst. *Journal of Materials Chemistry A*. 2015;**3**:1841-1846. DOI: 10.1039/c4ta06149g

[16] Xu M, Chai B, Yan J, Wang H, Ren Z, Paik K-W. Facile synthesis of fluorine doped graphitic carbon nitride with enhanced visible light photocatalytic activity. *Nano*. 2016;**11**:1650137. DOI: 10.1142/S179329201650137X

[17] Yuan B, Chu Z, Li G, Jiang Z, Hu T, Wang Q, et al. Water-soluble ribbon-like graphitic carbon nitride (*g-C₃N₄*): Green synthesis, self-assembly and unique optical properties. *Journal of Materials Chemistry C*. 2014;**2**: 8212-8215. DOI: 10.1039/c4tc01421a

[18] Patnaik S, Sahoo DP, Parida K. An overview on Ag modified *g-C₃N₄* based nanostructured materials for energy and environmental applications. *Renewable and Sustainable Energy Reviews*. 2018;**82**:1297-1312. DOI: 10.1016/j.rser.2017.09.026

[19] Majeed I, Manzoor U, Kanodarwala FK, Nadeem MA, Nadeem MA, Hussain E, et al. Pd-Ag decorated *g-C₃N₄* as an efficient photocatalyst for hydrogen production from water under direct solar light irradiation. *Catalysis Science & Technology*. 2018;**8**:1183-1193. DOI: 10.1039/c7cy02219k

[20] Han Q, Hu C, Zhao F, Zhang Z, Chen N, Qu L. One-step preparation of iodine-doped graphitic carbon nitride nanosheets as efficient photocatalysts for visible light water splitting. *Journal of Materials Chemistry A*. 2015;**3**: 4612-4619. DOI: 10.1039/c4ta06093h

[21] Zheng Y, Liu J, Liang J, Jaroniec M, Qiao SZ. Graphitic carbon nitride materials: Controllable synthesis and applications in fuel cells and photocatalysis. *Energy & Environmental Science*. 2012;**5**: 6717-6731. DOI: 10.1039/c2ee03479d

[22] Deonikar VG, Koteswara Reddy K, Chung WJ, Kim H. Facile synthesis of *Ag₃PO₄/g-C₃N₄* composites in various solvent systems with tuned morphologies and their efficient photocatalytic activity for multi-dye degradation. *Journal of Photochemistry and Photobiology A: Chemistry*. 2019;**368**:168-181. DOI: 10.1016/j.jphotochem.2018.09.034

[23] Liu T, Wang L, Lu X, Fan J, Cai X, Gao B, et al. Comparative study of the photocatalytic performance for the degradation of different dyes by *ZnIn₂S₄*: Adsorption, active species, and pathways. *RSC Advances*. 2017;**7**: 12292-12300. DOI: 10.1039/c7ra00199a

[24] Liang Q, Li Z, Huang ZH, Kang F, Yang QH. Holey graphitic carbon nitride nanosheets with carbon vacancies for highly improved photocatalytic hydrogen production. *Advanced Functional Materials*. 2015;**25**: 6885-6892. DOI: 10.1002/adfm.201503221

[25] Shi L, Li DQ, Li SF, Wang JR, Evans DG, Duan X. Structure, flame retarding and smoke suppressing properties of Zn-Mg-Al-CO₃ layered double hydroxides. *Chinese Science Bulletin*. 2005;**50**:1101-1104. DOI: 10.1360/04wb0043

[26] Jabeen M, Ishaq M, Song W, Xu L, Deng Q. Synthesis of Ni/Co/Al-layered

- triple hydroxide@brominated graphene hybrid on nickel foam as electrode material for high-performance supercapacitors. *RSC Advances*. 2017;7: 46553-46565. DOI: 10.1039/c7ra08744f
- [27] Zhang F, Du N, Li H, Liang X, Hou W. Sorption of Cr(vi) on Mg-Al-Fe layered double hydroxides synthesized by a mechanochemical method. *RSC Advances*. 2014;4:46823-46830. DOI: 10.1039/c4ra07553f
- [28] Hobbs C, Jaskaniec S, McCarthy EK, Downing C, Opelt K, Güth K, et al. Structural transformation of layered double hydroxides: An in situ TEM analysis. *npj 2D Materials and Applications*. 2018;2:1-10. DOI: 10.1038/s41699-018-0054-6
- [29] Mohapatra L, Parida K. A review on the recent progress, challenges and perspective of layered double hydroxides as promising photocatalysts. *Journal of Materials Chemistry A*. 2016; 4:10744-10766. DOI: 10.1039/c6ta01668e
- [30] Qu J, He X, Li X, Ai Z, Li Y, Zhang Q, et al. Precursor preparation of Zn-Al layered double hydroxide by ball milling for enhancing adsorption and photocatalytic decoloration of methyl orange. *RSC Advances*. 2017;7: 31466-31474. DOI: 10.1039/c7ra05316a
- [31] Dvininov E, Ignat M, Barvinschi P, Smithers MA, Popovici E. New SnO₂/MgAl-layered double hydroxide composites as photocatalysts for cationic dyes bleaching. *Journal of Hazardous Materials*. 2010;177:150-158. DOI: 10.1016/j.jhazmat.2009.12.011
- [32] Seftel EM, Mertens M, Cool P. The influence of the Ti⁴⁺ location on the formation of self-assembled nanocomposite systems based on TiO₂ and Mg/Al-LDHs with photocatalytic properties. *Applied Catalysis B: Environmental*. 2013;134-135:274-285. DOI: 10.1016/j.apcatb.2013.01.032
- [33] Dutta K, Das S, Pramanik A. Concomitant synthesis of highly crystalline Zn-Al layered double hydroxide and ZnO: Phase interconversion and enhanced photocatalytic activity. *Journal of Colloid and Interface Science*. 2012;366: 28-36. DOI: 10.1016/j.jcis.2011.09.081
- [34] Bhuvanewari K, Palanisamy G, Pazhanivel T, Maiyalagan T, Bharathi G. Photodegradation activity of nitrogen-rich graphitic carbon nitride intercalated ZnO\Mg-Al layered double hydroxide ternary nanocomposites on methylene blue dye. *ChemistrySelect*. 2019;4: 2982-2990. DOI: 10.1002/slct.201900146
- [35] Saravanan R, Aviles J, Gracia F, Mosquera E, Kumar V. International journal of biological macromolecules crystallinity and lowering band gap induced visible light photocatalytic activity of TiO₂/CS (chitosan) nanocomposites. *International Journal of Biological Macromolecules*. 2018;109: 1239-1245. DOI: 10.1016/j.ijbiomac.2017.11.125
- [36] Li W, Wang X, Wang Z, Meng Y, Sun X, Yan T, et al. Relationship between crystalline phases and photocatalytic activities. *Materials Research Bulletin*. 2016;83:259-267. DOI: 10.1016/j.materresbull.2016.06.021
- [37] Liu J, Lv G, Gu W, Li Z, Tang A, Mei L. A novel luminescence probe based on layered double hydroxides loaded with quantum dots for simultaneous detection of heavy metal ions in water. *Journal of Materials Chemistry C*. 2017;5:5024-5030. DOI: 10.1039/c7tc00935f
- [38] Qi Y, Liang Q, Lv R, Shen W, Kang F, Huang Z. Synthesis and photocatalytic activity of mesoporous g-C₃N₄/MoS₂ hybrid catalysts. *Royal Society Open Science*. 2018:2-10
- [39] Tonda S, Kumar S, Bhardwaj M, Yadav P, Ogale S. G-C₃N₄/NiAl-LDH

- 2D/2D hybrid heterojunction for high-performance photocatalytic reduction of CO₂ into renewable fuels. *ACS Applied Materials & Interfaces*. 2017;**10**: 2667-2678. DOI: 10.1021/acsami.7b18835
- [40] Chen J, Sheng Y, Song Y, Chang M, Zhang X, Cui L, et al. Multimorphology mesoporous silica nanoparticles for dye adsorption and multicolor luminescence applications. *ACS Sustainable Chemistry & Engineering*. 2018;**6**: 3533-3545. DOI: 10.1021/acssuschemeng.7b03849
- [41] Sobhana L, Sarakha M, Prevot V, Fardim P. Layered double hydroxides decorated with Au-Pd nanoparticles to photodegrade Orange II from water. *Applied Clay Science*. 2016;**134**:120-127. DOI: 10.1016/j.clay.2016.06.019
- [42] Indrasekara S, Kottegoda N. Synthesis and characterisation of exfoliated layered double hydroxide (LDH)/sugar nanocomposites. *Journal of the National Science Foundation of Sri Lanka*. 2011;**39**:113-119. DOI: 10.4038/jnsfsr.v39i2.3171
- [43] Wysocka J, Krakowiak S, Ryl J. Evaluation of citric acid corrosion inhibition efficiency and passivation kinetics for aluminium alloys in alkaline media by means of dynamic impedance monitoring. *Electrochimica Acta*. 2017;**258**:1463-1475. DOI: 10.1016/j.electacta.2017.12.017
- [44] Tan XF, Liu YG, Gu YL, Liu SB, Zeng GM, Cai X, et al. Biochar pyrolyzed from MgAl-layered double hydroxides pre-coated ramie biomass (*Boehmeria nivea* (L.) gaud.): Characterization and application for crystal violet removal. *Journal of Environmental Management*. 2016;**184**: 85-93. DOI: 10.1016/j.jenvman.2016.08.070
- [45] Vinayan BP, Zhao-Karger Z, Diemant T, Chakravadhanula VSK, Schwarzbürger NI, Cambaz MA, et al. Performance study of magnesium-sulfur battery using a graphene based sulfur composite cathode electrode and a non-nucleophilic Mg electrolyte. *Nanoscale*. 2016;**8**:3296-3306. DOI: 10.1039/c5nr04383b
- [46] Xu J, Gai S, He F, Niu N, Gao P, Chen Y, et al. A sandwich-type three-dimensional layered double hydroxide nanosheet array/graphene composite: Fabrication and high supercapacitor performance. *Journal of Materials Chemistry A*. 2014;**2**:1022-1031. DOI: 10.1039/c3ta14048b
- [47] Shinde SS, Sami A, Lee JH. Electrocatalytic hydrogen evolution using graphitic carbon nitride coupled with nanoporous graphene co-doped by S and Se. *Journal of Materials Chemistry A*. 2015;**3**:12810-12819. DOI: 10.1039/c5ta02656c
- [48] Petit M, Michez L, Raimundo JM, Malinowski T, Dumas P. An introduction to photocatalysis through methylene blue photodegradation. *European Journal of Physics*. 2016;**37**: 1-11. DOI: 10.1088/0143-0807/37/6/065808
- [49] Bhuvaneshwari K, Palanisamy G, Pazhanivel T, Bharathi G, Nataraj D. Photocatalytic performance on visible light induced ZnS QDs-MgAl layered double hydroxides hybrids for methylene blue dye degradation. *ChemistrySelect*. 2018;**3**:13419-13426. DOI: 10.1002/slct.201803183
- [50] Moussa H, Chouchene B, Mozet K, Schneider R, Gries T, Medjahdi G, et al. Growth of ZnO nanorods on graphitic carbon nitride gCN sheets for the preparation of photocatalysts with high visible-light activity. *ChemCatChem*. 2018;**10**:1-12. DOI: 10.1002/cctc.201801206
- [51] Saravanan R, Sacari E, Gracia F, Khan MM, Mosquera E, Gupta VK.

Conducting PANI stimulated ZnO system for visible light photocatalytic degradation of coloured dyes. *Journal of Molecular Liquids*. 2016;221:1029-1033. DOI: 10.1016/j.molliq.2016.06.074

[52] Cheng YH, Huang Y, Kanhere PD, Subramaniam VP, Gong D, Zhang S, et al. Dual-phase titanate/Anatase with nitrogen doping for enhanced degradation of organic dye under visible light. *Chemistry - A European Journal*. 2011;17:2575-2578. DOI: 10.1002/chem.201002256

[53] Teeparthi SR, Awin EW, Kumar R. Dominating role of crystal structure over defect chemistry in black and white zirconia on visible light photocatalytic activity. *Scientific Reports*. 2018;8:1-11. DOI: 10.1038/s41598-018-23648-0

[54] Salama A, Mohamed A, Aboamera NM, Osman TA, Khattab A. Photocatalytic degradation of organic dyes using composite nanofibers under UV irradiation. *Applied Nanoscience*. 2018;8:155-161. DOI: 10.1007/s13204-018-0660-9

[55] Azeez F, Al-Hetlani E, Arafa M, Abdelmonem Y, Nazeer AA, Amin MO, et al. The effect of surface charge on photocatalytic degradation of methylene blue dye using chargeable titania nanoparticles. *Scientific Reports*. 2018; 8:1-9. DOI: 10.1038/s41598-018-25673-5